

A multi-scale approach interpreting sediment processes and distribution from desert sand colour in central Saudi Arabia.

Andrew V Bradley^{1, 2}

Sue J McLaren²

Ahmed Al-Dughairi³

Nadia R Khalaf⁴

¹ Faculty of Engineering, Nottingham Geospatial Institute, Innovation Park, Jubilee Campus, Nottingham, NG7 2TU

² Department of Geography, University of Leicester, Leicester. LE1 7RH, UK.

³ Qassim University, Almulyda, Qaseem, Saudi Arabia.

⁴ University of Exeter, College of Social Sciences and International Studies, Institute of Arab and Islamic Studies, Exeter, Devon, EX4 4QJ, UK.

Corresponding Author: Andrew V Bradley

Address: Faculty of Engineering, Nottingham Geospatial Institute, Innovation Park, Jubilee Campus, Nottingham, NG7 2TU

Telephone: ++44 (0)115 846 6026

E mail: avbradley4@gmail.com

Key words: redness, sand sea, dust, iron oxide, Landsat

This article has been accepted for publication and undergone full peer review but has not been through the copyediting, typesetting, pagination and proofreading process which may lead to differences between this version and the Version of Record. Please cite this article as doi: 10.1002/esp.4438

Abstract

In central Saudi Arabia the redness of sands observed on satellite imagery, often related to iron oxide amount, was used to better interpret geomorphic processes operating in the area.

To compare variations between dune and interdune morphology, linear and dome dunes, and an ephemeral river partly buried under the sand sea, Nafud Al-Thuwayrat, a multiscale approach was used to identify the spatial variation in causes of iron oxide amounts and colour. Macro-scale mapping of Image Spectral Redness identified that the extent and intensity of colour grading across the orientation of well-defined linear and dome dune types, interdunes and the Wadi Al-Rimah, indicated sediment mixing of different provenance.

Meso-scale chemical, physical and colour analysis of surface samples indicated that iron oxide coated grains were present within all the samples and was not the sole control on Image

Spectral Redness. The reddest sediments were the best sorted medium-to fine-quartz sands with iron oxide bearing chemistry and the paler sediments contained coarser sands with additional feldspars, calcite and gypsum. Micro-scale analysis of grain characteristics found dune-interdune contrasts and that the reddest sands with iron coatings were of aeolian origin and the paler sands contained larger fluvial material mixed with reworked aeolian deposits.

Dust in the area consists of high amounts of iron oxide and appears to be a major contributor to redness in the sand dunes. These controls on colour show the sand seas are paler westwards because a major river and local drainage systems deliver fluvial sediments from the carbonate and sandstone bedrock into the quartz rich aeolian material from the linear dunes. Evaporite deposits dominate in the paler interdunes, and south of the Wadi the dome dunes are the reddest as they are not migrating but building up. This multiscale approach has provided a modern analogy of processes for palaeoenvironmental studies.

Introduction

In sandy deserts, it has been argued that surface colour gradients or redness caused by iron oxides, may indicate weathering, transpiration and sand sea age (Warren, 2013). Interpreting the processes that caused these colours can assist in the reconstruction of past and present environmental conditions (e.g. Muhs, 2004; Roskin *et al.*, 2012). Satellite images offer a valuable tool to interpret this colour change on macro-scales (e.g. White *et al.*, 2001; White *et al.*, 2007; Levin *et al.*, 2007; Roskin *et al.*, 2012; Scheidt *et al.*, 2011) assuming colour defining processes are uniform over large spatial scales. However, at the smaller meso- and micro-scales several chemical and physical processes operate (Prestel *et al.*, 1980; El Baz, 1980, McKee *et al.*, 1979) that influence the amount of iron oxide coating quartz sand grains (Van Houten, 1973; Folk, 1976). Evidence in stratigraphic profiles (e.g. Gardner & Pye, 1981) shows that dune reddening is not necessarily a unidirectional process (Folk, 1976) but also linked to age and depth (Folk, 1976; Bowman, 1982). Colour transitions are interrupted due to a different provenance (Roskin *et al.*, 2012) and there are reversals in redox reactions where waterlogging occurs (Levin *et al.*, 2007). Aeolian transport can also have opposite effects, on one hand, iron-bearing clay minerals can gradually be abraded from sand grains, especially larger grains (Krinsley & Doornkamp, 1972), causing a downwind reduction in the intensity of redness (Muhs & Holliday, 2001; Bullard & White, 2005; White & Bullard, 2009); on the other hand, transport can intensify redness because as sand grains are abraded into smaller grains the ratio of grain size and surface area for iron oxide coatings to accumulate on in the long term increases (Walker, 1979). Additionally, iron-rich lithology, such as weathered sandstones (Pye, 1983) may introduce an iron oxide plume into the transport pathway, and airborne dust containing iron oxides (Duce & Tindale, 1991; Cwiertny *et al.*, 2008; Shi *et al.*, 2012) from continental weather systems (Warren 2013) can locally deposit into the sediment mix. Many remote sensing studies of colour have been made in

coastal areas where the sand stocks are easily identified and discriminated as mixing between marine and terrestrial sources and the uniform scaling of reddening processes may be acceptable (e.g. White *et al.*, 2001; White *et al.*, 2007; Levin *et al.*, 2007; Roskin *et al.*, 2012; Scheidt *et al.*, 2011). However, as inland sand transport corridors combine with materials from different provenances (e.g. Pye, 1983), there must be subsequent mixing and reworking of sediment in the direction of sand transport. Interpretation of iron oxide accumulations from macro-scale observations therefore require a more detailed spatial understanding of the sand composition from the meso- and micro-scale.

Research identifying and interpreting sand colour has used a range of techniques across macro-, meso-, and micro-scales (Table 1). At the macro-scale, satellite remote sensing covers vast areas across challenging desert environments. When reflectance data at the macro-scale is coupled with ground observations on smaller scales, quantitative geochemical mapping is possible (e.g. White *et al.*, 2001; Bullard & White, 2002). Techniques include, spectral mixture modelling to extrapolate amount and extent of different minerals (White *et al.*, 1997; White *et al.*, 2007; Scheidt *et al.*, 2011) and the use of unitless spectral indices (Mathieu *et al.*, 1998; Bullard & White, 2002; Levin *et al.*, 2007; Roskin *et al.*, 2012) to map iron oxide amounts. Iron oxide amounts can be mapped as these indices have been correlated to the depth and wavelength of an absorption feature in the visible spectrum at ~540 nm (Bullard & White, 2002; Ben-Dor *et al.*, 2006) caused by the Fe³⁺-O charge transfer (Hunt *et al.*, 1971). Furthermore, indices produce continuous scales that improve on mapping against discrete categories such as Munsell colour (Bullard & White, 2002). At the smaller scales, meso-scale observations of sand may be from Munsell colour (e.g. Anton & Ince, 1986), spectroscopy (e.g. Ben-Dor *et al.*, 2006; Crouvi *et al.*, 2006; Bullard & White, 2002; Roskin *et al.*, 2012; Scheidt *et al.*, 2011), measurement of particular chemistry such as iron oxide amounts (e.g. Bullard & White, 2002) or calcium carbonate (e.g. White *et al.*, 2001) and

micro-scale analysis using a low power microscope, and a Scanning Electron Microscope (SEM) with Energy Dispersive X-rays (EDX; e.g. Pye, 1983). Detailed synoptic overviews of colour and process are rare, particularly using all three scales (e.g. White and Bullard, 2009) and even so sampling designs have created morphologically and spectrally selective data extrapolating over process detail. Restrictions have included collecting samples from dune crests to avoid differences in particle sorting (White *et al.*, 2001), dune faces that are illuminated on the satellite imagery (White *et al.*, 2007), and omitting morphology, such as interdunes, categorised as spectral anomalies because of vegetation and paleosols (Ben-Dor *et al.*, 2006). Importantly, these sampling strategies have excluded evidence for meso-scale sorting and deposition and micro-scale mineralogy that may influence colour, and importantly the conditions in interdunes between the dunes which can also be non-depositional, wet or dry (Lancaster, 1995).

In the study area the history of sand sea evolution is vague (Vincent, 2008) and little is known about past and present environmental conditions (McLaren *et al.*, 2009). This research provides an opportunity to gather and interpret evidence of geomorphic processes occurring in a landlocked sand sea. Within the present day regional north to north easterly seasonal ‘Shamal’ winds (Whitney *et al.*, 1983) there is a variation in dune type (McKee, 1979), as well as the presence of ephemeral subaerial and buried fluvial activity (Al-Sulaimi & Pitty, 1995), topped with processes between dunes and interdunes (Lancaster, 1995). With these spatial variations, assuming scale interchangeability and using a ‘one size fits all’ explanation for colour change at the macro-scale will erroneously explain any transitions in the geomorphic processes operating at the meso- and micro-scale. The aim of this work is to use a detailed multiscale approach with improved sampling to gather evidence for the extent and spatial complexity of reddening processes to interpret the mixing and working of sediments and describe recent and current geomorphic processes in the landscape. The objectives are to

identify: how macro-scale colour is impacted by mixing and sorting of different provenance using the support of meso- and micro-scale evidence; how the prediction of iron oxides from the reflectance spectra of images is impacted by multiple provenance and dune form; and if any other properties of the sands can be deduced from colour.

Study Area

The study location in central Saudi Arabia is between 26°05'N and 27°20'N and 44°05' E and 45°05'E an area of approximately 300 km² (Fig. 1). It is a good position to gain an understanding of the relationship between fluvial activity originating in the mountains of the Arabian Shield to the south west and aeolian activity between two major sandy areas, An Nafud to the north and the Rub' al Khali to the south (Fig. 1 (a)). The dominant drainage across the study site is the Wadi Al-Rimah – Al-Batin network, beginning on the Arabian shield east of Medinah and finishing north of the Persian Gulf in Kuwait (Al-Sulaimi & Pitty, 1995; El-Baz & Al-Sawari, 1996). There are variations in sand colour on the satellite image with the paler sands in the central west and the reddest sand generally to the east with localised alternations of colour across the dunes and interdunes (Fig. 1 (b)). The geology comprises a series of Palaeozoic and Mesozoic sandstone, claystone and limestone beds that generally strike in an arc from west-north-west to north-west and dip less than a degree towards the north-east (Vaslet *et al.*, 1985; Manivit, *et al.*, 1986). The stacking of these geological beds forms a series of cuestas and linear depressions. Ribbons of sandy desert (or nafud: an Arabic term for an erg or a sand sea), trace these topographic depressions and as the nafuds run through the study area they bury the bed of Wadi Al-Rimah. The general sequence of exposed surface geology, or potential source rocks, and nafuds eastwards along the Wadi Al-Rimah (Fig. 1 (c)) is, the Saq Formation (red sandstones), Sarah Formation (sandstone), the Khuff Formation and Sudair shales (limestone and gypsum) that dip to form the depressions filled by Nafud As Sirr (recent sand). The Jilh Formation (sandstones) and the

Minjur Sandstone dip under the Nafud Al-Mazhur and Nafud Al-Thuwayrat (recent sand).

Finally, the Marrat (sandstone), Tuwaiq Mountain Limestone and Hanifa Formation (limestone) surface between Nafud Thuwayrat and Nafud Sebah. Detailed descriptions of these units can be found in Powers *et al.*, (1996) and Al-Welaie *et al.*, (1985).

In these nafuds the dune type varies. Linear dunes hundreds of kilometres long exist in a high organisational state (Telfer & Hesse, 2013) and originate from the An Nafud north-west of the study area forming the morphology of the Nafud Al-Mazhur. There is then a morphological transition in the linear dunes at about the location of the buried Wadi Al-Rimah into rounded dome dunes approximately 1 to 2 km in diameter (McKee, 1979) that constitute the main body of the Nafud Al-Thuwayrat. A small arm in the east forms the Nafud Sebah where the dome dunes gradually deteriorate into isolated dune forms. Nafud Al-Thuwayrat merges into the next nafud and continues south as a conduit of sediment to the Rub' al Khali. The accumulation of the sands in the depressions between the cuestas determines that eastward draining wadis on the adjacent bedrock surfaces form ephemeral lakes (sabkhas) and clay-silt pans (khabras) against the west sides of the nafuds. The seasonal northerly 'Shamal' winds are thought to dominate and drive the sand transport trajectory from the An Nafud southwards through the study area, although weak westerlies can occur between seasons (Whitney *et al.*, 1983). Recent evidence shows another potential iron-rich source from the entrainment and deposition of dust which can occur at any time in the year (e.g. Alharbi *et al.*, 2013; Notaro *et al.*, 2013) from many directions (e.g. Draxler *et al.*, 2001; Cornforth, 2013; Yu *et al.*, 2013).

Method

Surface samples, no more than a centimetre depth, were taken from the centre of and as near to a spectrally uniform area of at least the size of a Landsat ETM+ pixel in the linear dune area (transect AB), the wadi area (CD) the dome dune areas (EFG), and across all three areas (HI) to represent different dune forms, a wide range of sand colours, and sediment transport directions. Samples were then taken to the laboratory and prepared accordingly for the following techniques:

Macro-scale.

A Landsat ETM+ image (Path 167, Row 042, 24/04/2002) was corrected geometrically, radiometrically (Campbell, 2002), and topographically to reduce the effect of shadowing on dunes (Tasumi *et al.*, 2000) with the ASTER GDEM method (Khalaf, 2012) and used to map the surface colour of the study area, by calculating Image Spectral Redness, (ImageSR; Bullard & White, 2002; see SI section 1).

Meso-scale.

(i) A portable spectroradiometer, FieldSpec3, was used to measure sample reflectance as ground verification to the satellite image (Bullard and White, 2002) and for the calculation of iron oxide absorption feature depth (Clark & Roush, 1984; Green & Craig, 1985). (ii) Samples were passed through a Horiba LA 950 particle size analyser and converted into phi (ϕ) units to measure particle size distribution range and characteristics of mean, dispersion (sorting range), skew and kurtosis (Friedman & Saunders, 1978). (iii) X-Ray Diffraction (XRD) was performed on milled samples with the Bruker D8 Advance with DaVinci XRD equipment to identify the sample mineralogy (e.g. Gardner 1983). (iv) To extract surface iron oxides from the sands (referred to here on as DiFe) each sample was treated with sodium

citrate and sodium dithionite (Mehra & Jackson 1960) and the residue was measured with an Atomic Absorption Spectrometer (AAS) Varian SpectrAA-200, to give the weight of iron oxide. (v) To calculate the percentage weight of CaCO_3 , each sample was treated using HCl (Loeppest & Suarez, 1996). (vi) Major chemical oxides were identified with X-ray fluorescence (XRF) using a PANalytical Axios-Advanced XRF spectrometer to assist in deductions of mineralogy using the principles of Mason & Moore (1982). (vii) Colour identification was made with Munsell colour charts (Munsell Colour Company, 1975) a useful benchmark to quantify sand colour (e.g. El Baz, 1980; Pye, 1983; Anton and Ince, 1986; Stokes & Breed, 1993; Walden & White, 1997; Bullard & White, 2002; Muhs, 2004; White & Bullard, 2005). Two analysts agreed on the correct classification as it is difficult to select the most visually dominant colour from an assortment of different coloured grains (Anton & Ince, 1986). Colour was recorded for the bulk samples and gently sieved sediment fractions representing: $> 2\text{mm}$ or $< \phi$ (phi) -1, (granules), 2mm to 1mm or ϕ -1 to 0 (very-coarse-sand); 1mm to 0.5mm or ϕ 0 to 1 (coarse-sand); 0.5mm to 0.25mm or ϕ 1 to 2 (medium-sand); 0.25mm to $125\mu\text{m}$ or ϕ 2 to 3 (fine-sand); $125\mu\text{m}$ to $62.5\mu\text{m}$ or ϕ 3 to 4 (very fine sand); $< 62.5\mu\text{m}$ or $> \phi$ 4 (silt and clay). The percentage occurrence of each colour per sediment fraction was then calculated. Samples of available sandstone bedrock sources (Jilh, Minjur and Saq sandstones) and airborne dust (from a storm, 1st May 2011) were also analysed by XRF and DiFe respectively to examine potential external iron sources. These quantitative data were then correlated with ImageSR at the scales of study area, dunes, interdunes and within individual transects.

Micro-scale

Samples were mounted, and gold coated for analysis with a Hitachi S-3600N Scanning Electron Microscope (SEM) to identify the nature of the samples and sorting characteristics as well as to identify the types and occurrence of mineral elements with the assistance of

Energy Dispersive X-rays (EDX) using an Oxford INCA 350 EDX system. Additional thin sections from the study area were also used to assess composition and characteristics of the sediments using a Nikon Eclipse LV100ND polarising microscope.

Results and analysis

Image analysis (macro-scale)

The ImageSR ratio varied between 0.401 and 0.535 and quantified the spatial complexity in colour and potential variation in iron oxide content across the study area (Fig. 2a). Within the gradual west to east increase in redness from the western Nafud Mahzur and the Wadi Al-Rimah to the Nafud Al-Thuwayrat and Nafud Sebalah the striping and mottling of colour shows localised colour changes which are caused by the presence of dunes and interdunes.

[Fig. 2]

The transect data emphasise this east to west colour transition, and that ImageSR can also be similar between and within the different geomorphic areas, dunes and interdunes (Fig. 2 (b)).

Different levels of aeolian activity marked by redness did not clearly separate out between dune types, more with spatial location within dune types. Ranking of these values found a strong east to west gradient across the north to south Shamal wind transport direction within the different nafuds (Table 2 SI). This highlights that the accretion of iron oxide by abrasion and sorting processes of the Shamal winds along the orientation of the dunes is combined with localised material of different provenance mixing into the iron coated sands in a west to east transport pathway.

Physical analysis (Meso-scale)

Particle size statistics in units of phi (ϕ) inversely correlated to a general reduction in mean grain size (R^2 0.2, $p < 0.001$) and a narrowing of sorting range with increasing ImageSR (R^2

0.4, $p < 0.001$). Similar analysis of kurtosis found a weak correlation (R^2 0.1, $p = 0.01$) with no significant correlation for median or skew. An inverse relationship of sorting range width and ImageSR is evident within each transect, with dunes generally better sorted than interdunes (Fig. 3 (a)). Two key sorting fractions were found to have opposing correlations to ImageSR. Fine sands (ϕ 2 to 3) are more positively correlated to ImageSR and coarse sands (ϕ 0 to 1) are more negatively correlated to ImageSR (Fig. 3 (b))

[Fig. 3]

The sorting profiles show the width and additionally the position of the sorting range within the grades of sand, granules and clays (Fig. 4). The dunes are generally moderately sorted medium to fine sands (ϕ 1 to 3) that are near symmetrical. The better sorted distributions, peaking with 10 to 20% of fine sands (ϕ 2 to 3) will have high ImageSR values compared to the flatter, skewed distributions when at least 10% peaks in the medium sands (ϕ 1 to 2). For the interdunes there is poor sorting over a wide range of grain sizes. The interdunes are often bimodal or have a shoulder on the distribution. With generally more coarse material in the profile e.g. peaking at 5 to 10 % with very coarse or coarse sands (ϕ -1 to 1) ImageSR values are low. However, ImageSR values of interdunes can be like dunes if there is peak of medium to fine sands (ϕ 1 to 3) with very few or no granules and coarse sands ($\phi < 0$). These patterns are found for each region (Fig. 4 (a-c)) and across the linear, wadi and dome transect (Fig. 4 (d)). The dust sample was found to have grain sizes between ϕ 0 and ϕ 10. Generally, the relationship of sorting into these greater percentages of fine sands (ϕ 2 to 3) and lower percentages of coarse sands (ϕ 0 to 1) correlates with higher ImageSR values across individual transects (Fig. 3 (b)).

[Fig. 4]

Colour estimates (Meso-scale)

The bulk samples (all fractions) show little variation in Munsell colour, generally 57% yellowish-red, (YR 5YR 5/6 - 5/8) with no pink (e.g. P 5YR 7/4) or reddish-brown (e.g. RB 5YR 5/4) colours. However, there is a greater range of Munsell colours when the samples are divided into different sorting fractions (Fig. 5). With decreasing grain-size there is a reduction or loss of the presence of pinks (e.g. PG 5YR 7/2, P 5YR 7/4), an increase in proportions of reddish-yellow (e.g. RY 5YR 6/6) then yellowish-red (e.g. YR 5YR 5/8) accompanied by a gradual increase in the red proportions (e.g. LR 2.5YR 6/6 plus R 2.5YR 5/8), and a greater likelihood of only containing the reddish browns and brown colours (e.g. LRB 5YR 6/4, RB 5YR 5/4 and B 7.5YR 5/4) in the finest fractions. The most abundant colour descriptions in the sand categories are reddish-yellow (RY) and yellowish-red (YR), rather than red (R) (SI Table 4). When compared to the sorting profiles (Fig. 4), leptokurtic (peaked) profiles concentrate sediment into specific sorting fractions with a narrow dispersion range. When this is mostly in the fine sand fractions (ϕ 2 – 3) the likelihood of containing sediment of a YR colour increases. Platokurtic (flatter) and bimodal profiles spread over more sorting fractions and when fractions are larger than the coarse sands ($\phi < 0$), have a wider range of colours including YR and RY and a mix of pinks (P and PG).

[Fig. 5]

Chemical analysis (meso-scale)

Mineralogy

XRD results found that the well sorted samples were dominated by silica, at least 95% quartz (SI Fig. 3). There was very little evidence for iron-bearing clay minerals or feldspars since the relevant peaks at 10-15 degrees and 27-30 degrees were too small to be statistically significant against a dominant quartz signature. An absence of background noise across the whole diffraction range caused by fluorescence of amorphous iron also suggested that there

were low undetectable amounts of iron that could not be confirmed (personal communication, Haidon C, 2013). It seems that haematite and goethite can be detected by XRD if there is a thick rim of iron oxide on the sample, capable of breaking above the XRD signature noise (e.g. Yuan *et al.*, 2015). XRD confirmed the presence of high proportions of silicate, additional mineralogy was inferred by observation and deduction from SEM, EDX, thin section work and the XRF major oxide chemistry.

Surface mineralogy (meso-scale)

DiFe iron oxide values were between 0.2 mg/L and 1.2 mg/L with an average of 0.51 mg/L. However, there was much more iron oxide, 8.96 mg/L, in the dust sample indicating another iron oxide source. It is acknowledged that DiFe analysis is susceptible to extraction of all iron oxides, including the red haematite, as demonstrated on loess (Lui *et al.*, 1995), and this may influence the concentration of iron oxide in the dust more than the sands. Nonetheless, the difference in iron oxide estimate from the dust is large and the sand samples from the XRD show large proportions of quartz-rich sand grains with minute, if any, clay minerals bearing iron oxide, (also supported by the SEM and EDX, see *micro-scale*). Thus, a large proportion of the DiFe detected iron oxides in the sands are from grain coatings. Contrary to previous studies (e.g. White *et al.*, 2001), it was difficult to confirm a clear and consistent association of DiFe iron oxide with ImageSR for the whole area (Fig. 6 (a)) and over the individual transects (SI Fig. 4). The percentage of carbonates was between 0.90 % and 24.59 % percent with an average of 4.09 % and standard deviation of 4.97. There was no clear correlation with ImageSR (SI Fig. 4). Greater amounts of CaCO₃ were recorded at the margins of the sand seas, transect AB, part F of EFG, along the wadi region in the centre of CD and around the wadi region of transect HI, suggesting a fluvial influx of carbonates from the local Marrat and Khuff geology. With an absence of a good correlation of iron oxide and CaCO₃ with ImageSR, linear regression techniques and mixture modelling to map accumulations surface

mineralogy at the macro-scale with ImageSR are likely to be highly uncertain and were not pursued.

[Fig. 6]

Sediment chemistry (meso-scale)

The XRF results of the local bedrock sources (SI Table 2) indicate a large source of SiO₂, a potential source of iron oxide from the Fe₂O₃, which may be haematite or goethite, and minor amounts within the clays and feldspars from the low concentrations of Al₂O₃, K₂O and Na₂O. In the nafuds, percentages were SiO₂ > 90 %, TiO₂ < 0.27 %, Al₂O₃ < 3.37%, Fe₂O₃ < 0.95 %, CaO < 4.36 %, Na₂O < 0.63 %, K₂O < 1.13 % with negligible amounts from the remaining oxides P₂O₅ and MnO, MgO and SO₃. A value of 99% quartz was measured in nearby Ad Dhana (Anton, 1984; 1993) and 94% in As Sirr (Garzanti *et al.*, 2013). Looking specifically at the groups that infer the presence of iron oxide bearing clays and iron oxide coatings that may cause redness, e.g. Fe₂O₃, Al₂O₃, and K₂O, a strong correlation with ImageSR is rare, sometimes inverse and varies transect by transect (SI Table 2). Only CaO and Na₂O have a consistent but inverse relationship to ImageSR suggesting that carbonates and sodium salts may influence the redness. Several of these oxides are also well correlated (SI Table 3). To simplify mineralogical inference and remove redundant information correlated oxides were grouped in round brackets ‘()’ and represented by an intuitive member in square brackets ‘[]’.

The correlated XRF groups were: ([Fe₂O₃], MgO and Ti₂O) ‘clay-iron’, evidence for iron rich mineralogy such as haematite, goethite, ilmenite etc. and clay minerals; ([Al₂O₃], Na₂O, K₂O) ‘clay-feldspars’, evidence for clay minerals, and feldspars from igneous and sedimentary prominence; CaO ‘calcite-gypsum’, as evidence for calcite and gypsum and; SiO₂ ‘silica’, as evidence of quartz. It was deduced that the CaO was largely a reflection of calcite and gypsum after eliminating the probability of Ca in clays and other carbonate minerals (see SI

Table 2 for explanatory notes and *micro-scale* analysis for details). The amounts of these XRF mineral groups also vary between each transect and have characteristic range in % w/v (Fig. 3 (c, d, e)). Correlations to ImageSR are poor except for a consistently weak inverse relationship to ‘calcite-gypsum’ in all transects (Fig. 3 (e)). However, when considered as a mix together and using a normalised ratio, the proportions of ‘clay-feldspars’ and ‘clay-iron’ to ‘calcite-gypsum’ become positively correlated to ImageSR (Fig. 6 (b)).

Spectral analysis (meso-scale)

The laboratory spectral analysis produced spectral signatures typical of sand samples (e.g. Bullard & White 2002; Ben-Dor *et al.*, 2006; Levin *et al.*, 2007; Roskin *et al.*, 2012). When convoluted to the Landsat wavebands and converted to LabSR produced a good proportional agreement with ImageSR (SI Fig.1) indicating any spectral conclusions drawn from the analysis of the laboratory samples should be a fair reflection of what the ImageSR portrays. The LabSR of the iron rich dust sample (0.459) was in the same range as the samples. Hull differencing found the absorption feature depth at ~540 nm in the visible part of the spectrum with depths of between 4.5% and 11.0%. Although the absorption feature depth increased with ImageSR as expected (Fig. 6 (c)), the relationship of feature depth was much better when considering a mix of the chemistry (Fig. 6 (b)) rather than with just surface iron oxides (Fig. 6 (a)).

Physical and mineralogical analysis (micro-scale)

Illustrated most strikingly between thin sections of dune sands and of interdunes sediments close to the buried wadi along transect CD there are distinct contrasts in sediment composition, characteristics, particle mixing and mineralogy. Dune sands are well rounded quartz grains with distinct uniform iron oxide rims coating the grains and occasional punctuations of thicker clay coatings (e.g. Fig. 7 (a)), whereas the inter-dune sands, close to

the buried wadi, contain the same characteristic iron coated quartz dune grains mixed amongst larger and smaller angular grains of feldspars, gypsum and calcite. There are fewer incidences of iron rims on all the clasts especially the more angular grains (e.g. Fig. 7 (b)).

[Fig. 7]

SEM analysis of transect samples confirmed the rounded morphology of dune sand grains found in the thin sections of the samples with the highest ImageSR on the dome dunes south of the buried Wadi (e.g. Fig. 8 (a)). The mineralogy of the dune samples was confirmed with EDX spectra as being mainly quartz, with bright patches on occasional grains as evidence of iron-coatings responsible for the red colour of silicate rich sands. Clay, calcite or gypsum grains are rare in these samples including a lack of evidence of feldspars. In these cases, we can deduce that the source of the XRF Fe_2O_3 mostly originates from iron oxide coatings found on the quartz sand grains. These iron-coated, rounded quartz sands have a moderately sorted peaked distribution (e.g. Fig. 8 (a)). At the other extreme, samples from interdunes with lower ImageSR near the buried wadi (e.g. Fig. 8 (b)) agree with the thin section findings (Fig. 7 (b)) showing that there is a mix of clast sizes, and degrees of roundness with a flatter bimodal sorting distribution. At this scale it was observed that there were clasts of calcium carbonate and CaSO_4 minerals as the major source for the CaO in the XRF. This confirmed that CaO did not solely reside on clay fragments. EDX spectra indicated a broader composition of quartz, feldspar, clays, and calcite grains. Many grains are coated with clay fragments and incidences of rounded iron-coated grains that are characteristic of the intermixed silicate rich dune sediment were present but rare. Although these two examples illustrate the extremes in sorting on dunes and interdunes, in the other SEM samples, depending on location, some dunes resembled sorting characteristics of interdunes, particularly in the wadi region, close to the western edges of the nafuds near the sabkahs, and in the dome dune region across the eastern side of transect HI across Nafud Al-Thuwayrat

(e.g. Fig. 8 (c)). In contrast, to the north of the buried Wadi, linear dunes on the east of transect AB across Nafud Al-Mazhur are better sorted quartz grains with iron oxide coatings and few clays (e.g. Fig. 8 (d)). These surface features, mineralogy and grain size characteristics are scaled into the illustrated meso-scale sorting profiles that determine the dominant Munsell colours (Fig. 5), and along with the XRF composition (Fig. 3) identify the spatial variation in colour controls in the transects and the overall spatial controls on ImageSR in the study area (Fig. 2).

[Fig. 8]

Discussion

A multi scale analysis has shown that in this study area, a 'one size fits all' explanation of colour and process was not feasible using macro-scale evidence alone. A better understanding of sand colour was possible with field knowledge utilising an improved and strong sampling strategy avoiding the exclusion of interdunes and spatial variations in sorting and mineralogy (Ben-Dor *et al.*, 2006; White *et al.*, 2001; 2007). Macro-, meso- and micro-scale observations in the study area revealed many of the samples across the transects contained more than just iron oxide coated quartz grains providing evidence that there were a range of different processes determining colour beyond the conventional colour interpretation (Bullard and White, 2005). Dependent on geomorphic location and processes operating there was a mix in different proportions of calcite, gypsum, feldspars and clays and airborne dust sources of different provenance. Understanding the spatial variation of these factors enabled a better interpretation of the landscape from sand sea colour.

At the macro-scale, the satellite imagery shows a base structure of well-defined linear, and dome dunes. The linear dunes reflect the sediment transport paths that are a result of the north westerly component of the Shamal winds (Fryberger *et al.*, 1984), the dome dunes form south

of the Wadi Al-Rimah. These sand dunes do not directly align with the overall divisions and gradation in ImageSR of the study area. According to Warren (2013) redness is a function of the amount of crystallised haematite in the grain coatings. The degree of redness does not completely correspond to the patterns of dunes and must be caused by the delivery of sediment from a range of different localised provenances which is reworked into the existing geochemistry (Whitney *et al.*, 1983; Anton & Ince, 1986; Garzanti *et al.*, 2013). To assume that ImageSR is detecting the change in concentration of iron oxide caused by abrasion and sorting on a homogenous substrate is now questionable, particularly as the imagery and field observations also found a variety of localised fluvial and evaporitic sediment sources feeding into the system. Nevertheless, the overall spatial changes in colour across the study area give a better indication on the extent, intensity, and probably more significantly, the activity of different geomorphic processes operating across the desert surface. Additionally, colour contrasts between dunes and interdunes, some of which contained Holocene paleolakes between the linear dunes (e.g. as McClure, (1976) identified in the Rub' al Khali) show that there are localised processes of sediment sorting within the wider sediment distribution and it was possible to identify sources of clay and evaporite salts from the positions of sabkha and khabra adjacent to the nafuds. Hence this general overview from ImageSR requires meso- and micro-scale evidence to piece together in more detail the range of processes operating. At the meso-scale, the correlation of ImageSR between the satellite images and the surface samples allowed a sounder interpretation into the causes of colour change measured on the imagery. Most surprisingly the measurement of iron oxide coatings (DiFe) did not correlate as well to ImageSR (Fig. 6 (a)) or the iron oxide absorption feature at ~540 nm (Fig. 6 (c)), central to the ImageSR calculation of Bullard and White (2005), supporting the idea that sand colour and ImageSR is influenced by material other than iron oxides. Although it has been found that the DiFe method can extract additional non-red iron minerals from fine materials

increasing the iron oxide estimate (Lui *et al.*, 1995) extensive covering or high incidences of iron oxide or iron bearing clays were rarely observed under the microscope. Moreover, many of the samples contained a mix of sediment other than iron coated silicates. The reflectance of calcite and gypsum is relatively high in the visible portion of the spectrum and will mask the depth of the iron oxide absorption feature. ImageSR calculations therefore cannot solely equate to the iron oxides (SI Table 1 and SI Fig. 2). This correlation of mixed sediments with the ImageSR calculation was consistent with the XRF data using the ratios of 'clay-feldspars' and 'clay-iron' to 'calcite-gypsum' (Fig. 6 (b)). Although mineralogy cannot be differentiated from XRF, many other minerals were inferred through use of the XRF groupings and evidence from the micro-scale analysis. Furthermore, the XRF results found that even if the amounts of potentially iron bearing 'clay-feldspar' and 'clay-iron' increase, a fairly small increase in amounts of 'calcite-gypsum' will counter any prediction of iron oxide concentration using ImageSR (Fig. 3 (d, e)). This outcome is supported by the work of Roskin *et al.*, (2012) who found that sand samples with higher amounts of calcite did not show a positive link with a redness index. Balsam *et al.*, (2014) conversely found that increasing calcite amounts can highlight the red coloured haematite in spectra. However, this was after these samples were milled, destroying any optical properties influenced by crystal structure, sorting, mixing and surface coatings found with *in situ* samples. Ben-Dor *et al.* (2006), working in a more wet coastal dune region, also highlighted that in interdune areas organic matter, chlorophyll (at around 680nm) and soil moisture would be problematic to spectra and elected to avoid predictions of interdune mineralogy. In the study area it was not necessary to treat interdunes in this way as they did not contain the density of vegetation found in coastal interdunes.

Sieving of dune and interdune samples into different phi sizes showed different colours were common in different sand fractions and that specific colours are emphasised dependant on

sorting profiles and sediment geochemical processes, therefore resulting in mixing of the different grains. This differentiation of colour was also found by Anton & Ince (1986) in several nafuds across Saudi Arabia. They concluded that, rather than age and aridity, local sediment colour in each sand field was affected by the nearby provenance of materials such as bedrock and alluvial soils, then subjected to their own variations of the colour determining processes.

Using the proportions of the XRF mineral groups with the grain size characteristics (Figs. 3, 4) the localised variations on colour due to spatial differences in provenance, transport pathways and processes of sorting and mixing is now recognised across the study area. At one extreme, the east of Transect AB, these results found that high ImageSR values tend to be fine grained silica rich sands (ϕ 2-3) iron oxide. Within the narrow sorting range Munsell colour analysis indicate this particle size tends to have an increasing probability of yellowish-red and reddish-yellow colours and is indicative of accumulation or abrasion of iron oxides caused by aeolian activity. At the other extreme, in the interdunes of CD, lower ImageSR values tend to have more coarse sand (ϕ 0-1) and less fine sand (ϕ 2-3) increasing the probability of reddish-yellow and pink material (Fig. 5). These samples are indicative of mixed provenance where geochemical carbonates and fluvial material combine with quartz and iron-rich aeolian material. With these two extremes a simple local synopsis of geomorphic processes can be built on. The east of transect AB is mainly a result of aeolian sorting and transport from a single northerly provenance, whereas CD and the west of AB is a mix of fluvial and aeolian material from multiple sources. EFG and HI, also with mixed sediments, are downwind of the Wadi and in the east show aeolian reworking as there is less 'calcite-gypsum' and increased amounts of finer grained iron coated quartz sand.

At the micro-scale, it was possible to determine mineralogy better than the XRD silica dominated signatures and deduce the contents of the XRF mineral groups from thin section,

SEM and EDX element spectra. The sands varied from highly uniform quartz grains to a broad mix of material including the highly reflective calcites and gypsum grains. Confirmed with the HCl analysis, this presence of carbonate minerals, supplied in greater quantities at the edges of the nafuds and along the wadi region by ephemeral drainage, indicates an influx of carbonates from the local Jurassic and Permian limestone geology. At this scale it was possible to see the presence and distribution of iron coating on the sediment clasts and how this related to the surrounding landscape. The variation in coatings was linked to the processes occurring on the linear and dome dunes, and between these dune types; within different locations of the dune form, i.e. dunes versus interdunes; between geomorphic locations, i.e. wadis versus palaeolakes, sabkha and khabra, dunes and interdunes. In terms of provenance of the iron coatings on the quartz sediment clasts, analysis identified that the redness is only present largely coating the rounded clasts. The sand grains were therefore rounded prior to the formation of a red coating. This is exactly the descriptions that Phillips (1882) and Warren (2013) have used to argue that the redness of sediments is from dust. The dust sample analysed contained 8.96 mg/L of iron oxide, several times greater than the average of the sand samples, 0.51 mg/L. This fine iron oxide rich material ($\phi > 5$) can be deposited and entrained anywhere and in areas that experience periods of relatively low energy and activity. It appears that dust accumulation is likely to intensify the redness of sands.

Sediment movement

Although there are basic models of sand origins in these sand seas, which are built on relatively regional sampling schemes (Whitney *et al.*, 1983; Anton and Ince, 1986; Garzanti *et al.*, 2013), our detailed transect method has highlighted that fluvial activity may be more influential on sediment mixing and control of dune types at more localised scales than previously considered. In Nafud Al-Mazhur (transect AB) the linear dunes deliver sediment

from the NNW via the 'Shamal' winds. On the east side, high ImageSR indicates that sediment is a homogenous and well sorted mainly quartz material which originates from the An Nafud as described by Garzanti *et al.*, (2013). On the west side of the sand sea even though the same dune forms and wind regimes persist over the landscape, lower ImageSR values are interpreted to indicate a more heterogeneous mix of sediment. Tracing northwards out the study area these dunes cross the local geology including a Devonian outcrop of the Jauf Formation, a calcareous siliclastic rock, and probably receive eastward drifting material from local nafuds on the Arabian shield to the west. This detailed analysis confirms suggestions that the central Arabian nafuds do have additional localised sources (Whitney *et al.*, 1983; Anton & Ince, 1986; Garzanti *et al.*, 2013).

In the study area, local sediment sources are also delivered via small wadis which have passed over the local sandstones, gypsum and limestone units. The larger Wadi Al-Rimah introduces sediments from further afield in the Arabian shield, as well as these local units (transect CD). In a regional overview, where previous sampling was located on the limits of this study area, choking of Wadi Al-Rimah by the sand seas may have blocked any detectable mineralogical input from the wadi to the sand seas (Garzanti *et al.*, 2013). This is not true in the immediate vicinity of the wadi-sand sea interface. At more localised scales fluvial activity is evident from ponding of surface water in the sabkhas and khabra, adjacent to the sand seas, segregating finer clays, silt and salts susceptible to transport as iron-rich dust across the sand seas by the weak westerly's that occur between the northerly 'Shamal' winds (Whitney *et al.*, 1983). There are also palaeolakes and evaporites in the interdune areas, likely to be fed by sub flows in choked wadis, like Al-Rimah, that can recharge groundwater from sub surface flows (Vincent, 2008). Collectively these localised processes contribute to the transition from paler and less well sorted sediments in the west with a heterogeneous mix of mineralogy to better sorted homogenous sands to the east sides of these sand seas.

The dune type transition from linear to the dome dune types coincide with the buried Wadi Al-Rimah. ImageSR shows that sorting and mixing properties of the sediment change downwind of that crossing point. Moving from west to east the fluvial material is being diluted in proportion to aeolian sediment, and on the east side where little fluvial material is present, the red aeolian sediment is better sorted and more homogenous in nature. In the linear dunes the lower ImageSR values infer there is more activity and abrasion of the sands in comparison to the dome dunes to the south of the Wadi Al-Rimah (Fig.2). Reduced aeolian activity in the domes causes sand accumulation allowing finer more red fractions to accumulate. Here the conditions for the incorporation of iron rich dust, from multiple directions and sources (Draxler *et al.*, 2001; Cornforth, 2013; Alharbi *et al.*, 2013; Notaro *et al.*, 2013; Yu *et al.*, 2013), are enhanced and unlike areas of greater sediment movement, a build-up can occur which will accentuate the red colour. Calculations of equivalent sand depth to the south east of the buried wadi in Nafud Al-Thuwayrat have found evidence that the sand is indeed accumulating in the reddest areas as it is deeper than the rest of the study area (Khalaf, 2012). In the interdunes dust is either moved away or diluted by evaporites and incoming wadi sediments. Whatever the mechanism, deposition of finer sands is favoured downwind of the Wadi Al-Rimah. Additionally, a change in moisture due to wetter clasts south of the Wadi may alter thresholds in aeolian transport processes, combined with a change in wind patterns, perhaps related to the strength of the westerlies (Whitney *et al.*, 1983) along the course of the Wadi Al-Rimah.

This multi-scale approach using ImageSR and ground observations has provided a modern analogy of the sediment sources and contributions of fluvial, aeolian and palaeolake accumulation processes including the scale, extent and outcomes of sediment distribution processes on these sand seas. In the Negev, Roskin *et al.*, (2012), found the sediment characteristics and the colour of stratigraphic profiles change with depth as tongues of

material, introduced from different provenances, switch through time. Evidence for the continuation of Wadi Al-Rimah into Kuwait (El-Baz & Al-Sawari, 1996) indicates that the Wadi system through Nafud Al-Thuwayrat has been more dominant in the past. To understand this ebb and flow between fluvial and aeolian processes, this modern colour signature should provide a better understanding for palaeoenvironmental reconstruction in the stratigraphic profile.

8. Conclusion

Sub-continental analysis with spot sampling of sand colour and mineralogy can overlook the subtleties of local mineralogical variations of inland sand seas. Given the duration of large scale dune forms, these localised perturbations reflect the superimposition of complex sediment mixing, composition and activity that may well be more informative indicators for palaeoenvironmental reconstruction. Interpreting colour from optical images and assuming equivalence between scales requires care. It is recommended to use caution with ImageSR unless meso- and micro-scale knowledge is considered in depth. This is most crucial where mixed provenance and sediment sorting can influence ImageSR in a way that will undermine age and distance of transport relationships (Warren 2013), conventionally interpreted as the amount of iron oxides present (e.g. Muhs & Holliday, 2001; Bullard & White, 2005; White & Bullard, 2009). Furthermore, the meso- and micro scale evidence found a strong case for dust as an intensifier of redness much as Phillips (1882) and Warren (2013) described from the iron coatings found on rounded grains. These findings have helped towards understanding sediment sources and patterns of sand movement in central Saudi Arabia.

Acknowledgements

Field work was supported by the government of Saudi Arabia to AA-D, SJM and AVB.

Thanks to Robert Ewers for the professional support given to AVB during ERC grant 281986 at Imperial College, the granting of academic study leave by the University of Leicester to SJM for scientific writing, Analytic UK for the loan of the ASD FieldSpec3 spectroradiometer, comments from the anonymous reviewers and Lil Dougie on an early manuscript of this paper. Satellite image, USGS Earth Explorer <http://earthexplorer.usgs.gov/>

last accessed: 25/07/14. ASTER GDEM, supplied by METI and NASA

(<http://gdem.ersdac.jspacesystems.or.jp/> last accessed: 25/07/14).

References

Al-Sulaimi, J.S., & Pitty, A.F. (1995). Origin and depositional model of Wadi al Batin and its associated alluvial fan, Saudi Arabia and Kuwait. *Sedimentary Geology*, 97, 209-229.

Al-Welaie, A. (1985). *Geology and Geomorphology of Saudi Arabia*. Al Obeikan Library. Riyadh, Saudi Arabia.

Alharbe, B.H., Maghrabi, A., & Tapper, N. (2013). The March 2009 dust event in Saudi Arabia. *Bulletin of the American Meteorological Society*, 94, 515–528. doi:

dx.doi.org/10.1175/BAMS-D-11-00118.

- Anton, D. (1984). Aspects of Geomorphological Evolution; Paleosols and Dunes in Saudi Arabia, 275-296. In: A.R. Jado & J.G. Zötl, (Eds.), *Quaternary Period in Saudi Arabia*, Vol. 2, Wien, Springer-Verlag
- Anton, D. (1993). Modern eolian deposits of the Eastern Province of Saudi Arabia, 365-378, In: M.E. Brookfield, & T.S. Ahlbrandt (Eds.), *Eolian Sediments and Processes, Developments in Sedimentology 38*, Amsterdam, Elsevier
- Anton, D., & Ince, F. (1986). A study of sand colour and maturity in Saudi Arabia. *Zeitschrift für Geomorphologie*, 30 (3), 339-356.
- Balsam W., Ji, J., Renock, D., Deaton, B.C., & Williams, E. (2014). Determining hematite content from NUV/Vis/NIR spectra: Limits of detection. *American Mineralogist*, 99, 2280-2291.
- Ben-Dor, E., Levin, N., Singer, A., Karnieli, A., Braun, O., & Kidron, G.J. (2006). Quantitative mapping of the soil rubification process on sand dunes using airborne hyperspectral sensor. *Geoderma*, 131, 1-21.
- Blount, G., Smith, M.O., Adams, J.B., Greeley, R., & Christensen, P.R. (1990). Regional Aeolian Dynamics and Sand Mixing in the Gran Desierto: Evidence from Landsat Thematic Mapper Images. *Journal of Geophysical Research*, 95, 15, 463-15, 482.
- Bowman, D. (1982). Iron coating in recent terrace sequences under extremely arid conditions. *Catena*, 9, 353-359.
- Bullard, J.E., & White, K. (2002). Quantifying iron oxide coatings on sand dunes using spectrometric measurements: An example from the Simpson-Strzelecki Desert, Australia. *Journal of Geophysical Research*, 107 No B6,2125, doi: 10.1029/2001JB000454.

Bullard, J.E., & White, K. (2005). Dust production and the release of iron oxides resulting from the aeolian abrasion of natural dune sands. *Earth Surface Processes and Landforms*, 30, 95-106.

Campbell, J.B. (2002). *Introduction to Remote Sensing*. 3rd Edition, Guilford Press, New York, pp 621.

Clarke, R.N., & Roush, T.L. (1984). Reflectance spectroscopy: Quantitative analysis techniques for remote sensing applications. *Journal of Geophysical Research*, 89, 6329-6340.

Cornforth, R.J. (2013). West African Monsoon 2012. *Weather*, 68(10), 256-263.

Crouvi, O., Ben-Dor, E., Beyth, M., Avigad, D., & Amit, R. (2006). Quantitative mapping of arid alluvial fan surfaces using field spectrometer and hyperspectral remote sensing. *Remote Sensing of Environment*, 104, 103-117.

Cwiertny, D.M., Baltrusaitis, J., Hunter, G.J., Laskin, A., Scherer, M.M., & Grassian, V.H. (2008). Characterization and acid-mobilisation study of iron containing mineral dust source materials. *Journal of Geophysical Research*, 113, D05202 doi: 1029/2007JD009332.

Draxler, R.R., Gillette, D.A., Kirkpatrick, J.S., & Heller, J. (2001). Estimating PM₁₀ air concentrations from dust storms in Iraq, Kuwait and Saudi Arabia. *Atmospheric Environment*, 35, 4315-4330.

Duce, R.A., & Tindale, N.W. (1991). Atmospheric transport of iron and its deposition in the ocean. *Limnology and Oceanography*, 36(8), 1715-1726.

El-Baz, F. (1980). Desert varnish on sand grains from the western desert of Egypt: Importance of clay component and implications to Mars. *Eleventh Lunar and Planetary*

Science Conference, Johnson Space Center, March 17-21. Lunar and Planetary Institute, Texas.

El-Baz, F., & Al-Sawari, M. (1996). Kuwait as an alluvial fan of a paleo-river. *Zeitschrift für Geomorphologie, Supplement band 103*, 49-59.

Fitzsimmons, K.E., Magee, J.W., & Amos, K.J. (2009). Characterisation of aeolian sediments from the Strzelecki and Tirari Deserts, Australia: Implications for reconstructing palaeoenvironmental conditions. *Sedimentary Geology*, 218, 61-73.

Folk, R.J. (1976). Reddening of desert sands: Simpson Desert, N.T. Australia. *Journal of Sedimentary Petrology*, 46(3), 604-615.

Friedman, G.M., & Saunders, J.E. (1978). *Principles of Sedimentology*, John Wiley and Sons, New York. pp792.

Fryberger S.G., Al Sari A.M., Clisham T.J., Rizoi, S.A.R., Al Hinai K.G. (1984) Wind sedimentation in the Jafarah sand sea, Saudi Arabia. *Sedimentology*, 31, 413-431.

Gardner, R. (1981). Reddening of dune sands – evidence from southeast India. *Earth Surface Processes and Landforms*, 6(5), 495-468.

Gardner, R. (1983). Reddening of tropical coastal dune sands. 103-115, In R.C.L. Wilson (Ed.), *Residual deposits: surface related weathering processes and materials*, Geological Society special publication N°11, Blackwell Scientific Publications, Oxford.

Gardner, R., & Pye, K. (1981). Nature, origin and paleoenvironmental significance of red coastal and desert dune sands. *Progress in Physical Geography*, 54, 514-534.

Garzanti, E., Vermeesch, P., Andó, S., Vezzoli, G., Valagussa, M., Allen, K., Kadi, K.H., Al-Juboury, A.I.A. (2013). Provenance and recycling of Arabian desert sand. *Earth Science Reviews*, 120, 1-19.

Green, A.A., & Craig, M.D. (1985). Analysis of aircraft spectrometer data with logarithmic residuals, in Proceedings of the Airborne Imaging Spectrometer Data Analysis Workshop, April, 1985, (G. Vane and A. Goetz, eds.) JPL Publication 86-35, 111-119.

Hunt, G.R., Salisbury, J.W., & Lenhoff, C.J. (1971). Visible and near-infrared spectra of minerals and rocks: III Oxides and hydroxides. *Modern Geology*, 2, 195-205.

Khalaf, N.R. (2012). Analysis of complex dune field patterns of the Qassim province Saudi Arabia using satellite remote sensing. *MSc Thesis*, University of Leicester UK.

Krinsley, D.H., & Doornkamp, K. (1972). Sand Grain Surface Textures. In W.C.Mahaney, (Ed.), *Atlas of Sand Grain Surface Textures and Applications*, 2002 Oxford University Press, Oxford.

Lancaster (1995). *Geomorphology of Desert Dunes*, Routledge, London. pp290

Leopert & Suarez (1996) Carbonate and Gypsum, In Soil Analysis. Part 3. Chemical Methods--SSSA Book Series no. 5. Chapter 15, 1272, 437-474. U.S. Department of Agriculture: Agricultural Research Service, Lincoln, Nebraska.

Levin, N., Tsoar, H., Maia, L.P., Claudino Sales, V., & Herrmann, H. (2007). Dune Whitening and inter-dune freshwater ponds in NE Brazil. *Catena*, 70 (1), 1-15.

Lui, X., Rolph, T., & Bloemendal, J. (1995). The Citrate-Biocarbonate-Dithionite (CBD) Removable Magnetic Component of Chinese Loess, *Quaternary Proceedings*, 4, 55-58.

Manivit, J., Vaslet, D., Berthiaux, A., Le Strat, P., & Fourniguet, J. (1986). Explanatory notes to the geological map of the Buraydah Quadrangle, Sheet 26G, Kingdom of Saudi Arabia.

Ministry of Petroleum and Mineral Resources, Jidda, Saudi Arabia.

Mason, B.H., & Moore, C.B. (1982). *Principles of Geochemistry*, Fourth Edition. Smith & Wylie intermediate geology series. John Wiley & Sons, New York. pp344.

Mathieu, R., Pouget, M., Cervelle, B., & Escadafal, R. (1998). Relationships between Satellite-Based Radiometric Indices Simulated Using Laboratory Reflectance Data and Typic Soil Color of an Arid Environment. *Remote Sensing of Environment*, 66, 17-28.

McClure, H.A. (1976) Radiocarbon chronology of the late-Quaternary lakes in the Arabian desert. *Nature* 263 (5580), 755-756.

McKee, E.D. (1979). A study of global sand seas. *U.S. Geological Survey professional paper*, 1052, Washington, pp429.

McLaren, S., Al-Juaidi, F., Millington, A.C., & Bateman, M.D. (2009). Evidence for wetter events in the arid interior of Central Saudi Arabia. *Journal of Quaternary Sciences*, 24(2), 198-207. doi: 10.1002/jqs.1199.

Mehra, O.P., & Jackson, M.L. (1960). Iron Oxide removal from soil and clay by a dithionite-citrate system buffered with sodium bicarbonate. *Clay and clay minerals*, 7, 317-327.

Muhs, D.R., & Holliday, V.T. (2001). Origin of late Quaternary dune fields on the Southern High Plains of Texas and New Mexico. *USGS Staff-Published Research*, University of Nebraska, Lincoln.

Muhs, D.R. (2004). Mineralogical maturity in dunefields of North America, Africa and Australia. *Geomorphology*, 59, 247-269.

Munsell Colour Company Inc. (1975). Munsell Soil Colour Charts. Baltimore Md.

Notaro, M., Alkolibi, F., Fadda, E., & Bakhrjy, F. (2013). Trajectory analysis of Saudi Arabian dust storms. *Journal of Geophysical Research: Atmospheres*, 118(12), 6028–6043, F
DOI: 10.1002/jgrd.50346.

Powers, R., Ramirez, L., Redmond, C., & Elberg, J. (1966). Geology of the Arabian Peninsula: Sedimentary geology of Saudi Arabia. *US Geological Survey Professional Paper*. United States Government Printing Office, Washington, D. C., pp147.

Prestel, D.J., & Wainwright, J.E. (1980). Studies of the coatings of sand grains from the Gilf Kebir, Southwest Egypt. In P. Wirth, W.R. Greely, & R. D'Alli (Eds.), *Reports of the Planetary geology Program, 1979-1980*. NASA Technical Memorandum 81776, NASA Office of Space Science, Washington D.C.

Phillips, J. A. (1882). The red sands of the Arabian Desert. *Quarterly Journal of the Geological Society London*. 38, 110–113.

Pye, K. (1981). Rate of dune reddening in a humid tropical climate. *Nature*, 290, 582-584.

Pye, K. (1983). *Post-depositional reddening of late Quaternary coastal dune sands, north-eastern Australia*. Geological Society, London, Special Publications v.11, 117-129. doi: 10.1144/GSL.SP.1983.011.01.13.

Roskin, J., Rozenstien, O., Blumberg, D.G., Tsoar, H., & Porat, N. (2012). Do dune sands redden with age? The case of the northwestern Negev dunefield, Israel. *Aeolian Research*, 5, 63-65.

Scheidt, S., Lancaster, N., Ramsey, M. (2011). Eolian dynamics and sediment mixing in the Gran Desierto, Mexico, determined from infrared spectroscopy and remote-sensing data.

Geological Society of America Bulletin, 123, 1628-1644. doi: 10.1130/B30338.1.

Shi, Z., Krom, M.D., Jickells, T.D., Bonneville, S., Carslaw, K.S., Mihalopoulos, N., Baker, A.R., & Benning, L.G. (2012). Impacts on iron solubility in the mineral dust by processes in the source region and the atmosphere: A review. *Aeolian Research*, 5, 21-42.

Stokes, S., & Breed, C.S. (1993). A chronostratigraphic re-evaluation of the Tusayan dunes, Moenkopi Plateau and southern Ward Terrace, northeastern Arizona. In K. Pye (Ed.), *The dynamics and environmental context of aeolian sedimentary systems*. London: Geological Society of London, Special Publication No. 72, 75-90.

Telfer, M.W., & Hesse, P.P. (2013). Paleoenvironmental reconstructions from linear dunefields: recent progress, current challenges and future directions. *Quaternary Science Reviews*, 78, 1-21.

Tusumi, M., Bastiannesen, W., & Allen, R.G. (2000). Appendix C: A Step-by-Step Guide to Running SEBAL. In A. Morse, M. Tasumi, R.G. Allen, & W.J. Kramber (Eds.), *Application of the SEBAL Methodology for Estimating Consumptive Use of Water and Streamflow Depletion in the Bear River Basin of Idaho through Remote Sensing*. Department of Water Resources. University of Idaho, Idaho, 79-107.

Van Houghton, F.B. (1973). Origin of red beds-a review: 1961-1972. *Annual Review of Earth and Planetary Sciences*, 1. 39-61.

Vaslet, D., Beurrier, M., Villey, M., Manivit, J., Le Strat, P., Le Nindre, Y-M., Berthiaux, A., Brosse, J-M., Fourniguet, J. (1985). Explanatory notes to the geological map of the Al

Faydah Quadrangle, Sheet 25G, Kingdom of Saudi Arabia. *Ministry of Petroleum and Mineral Resources*, Jidda, Saudi Arabia.

Vincent, P. (2008) Saudi Arabia. An Environmental Overview. Taylor and Francis, London. pp 309

Walden, J., & White, K. (1997). Investigation of the controls on dune colour in the Namib Sand Sea using mineral magnetic analysis. *Earth and Planetary Science Letters*, 152, 187-201.

Walden, J., White, K.H., Kilcoyne, S.H., & Bentley, P.M. (2000). Analysis of iron oxide assemblages within Namib dune sediments using high field remanence measurements (9 T) and Mössbauer analysis. *Journal of Quaternary Science*, 15(2), 185-195.

Walker, T.R. (1979). Red colour in aeolian sand. In E.D. McKee (Ed.), *A study of Global Sand seas*. USGS Professional Paper vol. 1052. pp 61-81.

Warren, A. (2013). *Dunes: Dynamics, Morphology, History*. RGS-IBG Book Series, Wiley-Blackwell, Chichester. pp240.

Wasson, R.J. (1983). Dune sediment types, sand colour, sediment provenance and hydrology in the Strzelecki-Simpson dunefield, Australia. In M.E. Brookfield & T.S. Ahlbrandt (Eds.), *Eolian sediments and processes*, pp165-195. Amsterdam, Elsevier.

White, K., & Bullard, J. (2009). Abrasion control on dune colour: Muleshoe Dunes, SW USA. *Geomorphology*, 105, 59-66.

White, K., Goudie, A., Parker, A., & Al-Farraj, A. (2001). Mapping the geochemistry of the northern Rub' al Khali using Multispectral remote sensing techniques. *Earth Surface Processes and Landforms*, 26, 735-748, doi: 10.1002.esp218.

White, K., Walden, J., Drake, N., Eckhardt, F., & Settle, J. (1997). Mapping the Iron Oxide Content of Dune Sands, Namib Sand Sea, Namibia, Using Landsat Thematic Mapper Data. *Remote Sensing of Environment*, 62, 30-39.

White, K., Walden, J., & Gurney, S.D. (2007). Spectral properties, iron oxide content and provenance of Namib dune sands. *Geomorphology*, 86, 219-229.

Whitney, J.W., Faulkender, D.J., Rubin, M. (1983) The environmental history and present condition of Saudi Arabia's northern sand seas. United States Department of the Interior Geological Survey, Open-File Report 83-749.

Yu, Y., Notaro, M., Liu, Z., Kalashnikova, O., Alkolibi, F., Fadda, E., & Bakhrjy, F. (2013). Assessing temporal and spatial variations in atmosphere dust over Saudi Arabia through satellite, radiometric, and station data. *Journal of Geophysical Research-Atmospheres*, 118, 13235-13264. doi: 10.1002/2013JD020677.

Yuan, L., Sun, L., Fortin, D., Wang, Y., Yin, X. (2015) Microscale characterisation and trace element distribution in Bacteriogenic ferromanganese coatings on sand grains from an intertidal zone of the East China Sea. *PlosOne*. Doi:10.1371/journal.pone.0119080

Table 1: Examples of research into sand redness and the methods used to measure redness or sand colour showing the combinations and different scales of analysis used. Mic., Mes., Mac., = Micro-, Meso-, and Macro-scale respectively

Paper	Location	Environment	General Study	Sampling	Mic.		Mes.						Mac.	Other relevant	
					Thin sections	SEM EDX	Munsell chart	XRD XRF	DiFe Magnetism	Particle size Size fractions	Spectroscopy	Remote image			
Gardner (1981) Gardner (1983)	SE India, Sri Lanka and the Natal	Coastal sands subject to high seasonal rainfall from either monsoon or summer rain	Pedogenesis in soil profiles	Stratigraphic	•	•	•	•							1
Pye 1983	NE Australia	Coastal dunes in the wet tropics	Pedogenesis in dune profiles	Stratigraphic		•	•	•	•		•				1, 3, 8
Wasson (1983) Simpson – Strzelecki desert, Australia		Inland dune system with some palaeolakes and creeks	Sediment transport and deposition in relation to colour ageing	Surface and stratigraphic profiles	•	•	•	•		•					
Anton and Ince (1986)	Saudi Arabia	Saudi Arabian sand seas	Provenance or process determining colour?	Archived samples			•				•				2
White <i>et al.</i> (1997)	Namib	Coastal to inland dune field containing ephemeral river, increasing moisture inland	Determine iron oxide concentrations	Along transect, forms unspecified						•				•*	
Walden and White (1997)	Namib	Coastal to inland dune field containing ephemeral river increasing moisture inland	Identify source materials causing colour	Along transect, forms unspecified			•			•				•*	
Walden <i>et al.</i> (2000)	Namib	Coastal to inland dune field containing ephemeral river increasing moisture inland	To identify Fe minerals and ascertain environmental controls on their formation	Along transect, forms unspecified						•				•*	3
White <i>et al.</i> (2001)	Rub ‘Al Khali, UAE.	Northern part of sand sea next to the coast	Geochemistry in relation to provenance and weathering	Top of active slip faces						•				•*	4
Bullard and White (2002)	Simpson – Strzelecki desert, Australia	Inland dune system with some palaeolakes and creeks	Surface colour and iron oxides	Surface dune crests			•			•				•	5
Muhs <i>et al.</i> (2001)	SW USA	Aeolian dunes near Colorado river	Contribution of river sediments to dunes in pathway of aeolian transport direction	Sub surface samples				•	•	•				•	
Muhs (2004)	Various, N America, Africa, Australia	Mainly inland dune fields with the exception of the Namib	Provenance and evolution of dunefields					•	•						

Figure 1.

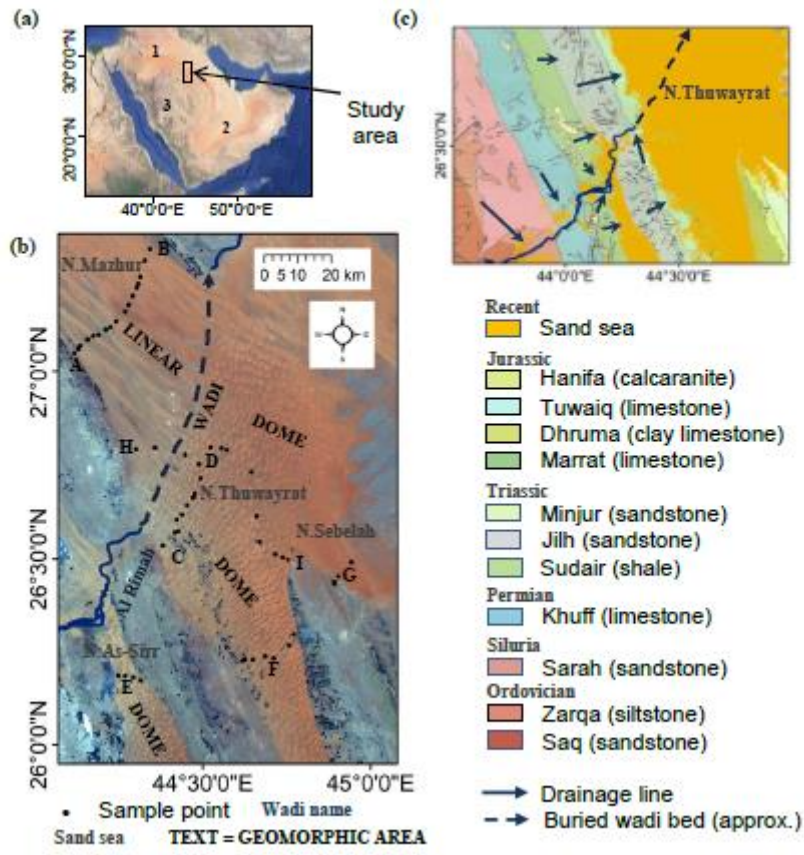


Fig.1. (a) Google map of the Saudi Arabian Peninsula showing the major sand seas, An Nafud (1) the Rub' Al Khali (2) and the Arabian Shield (3), in relationship to the study area, (b) Landsat ETM+ satellite image (Bands R3, G2, B1) showing the colour variation of the study area, sample and transect locations, and geomorphic areas used in the analysis. (c) Generalised synopsis of exposed major geological units (Manivit *et al.*, 1986) with sand sea cover and surface drainage (arrows).

Figure 2

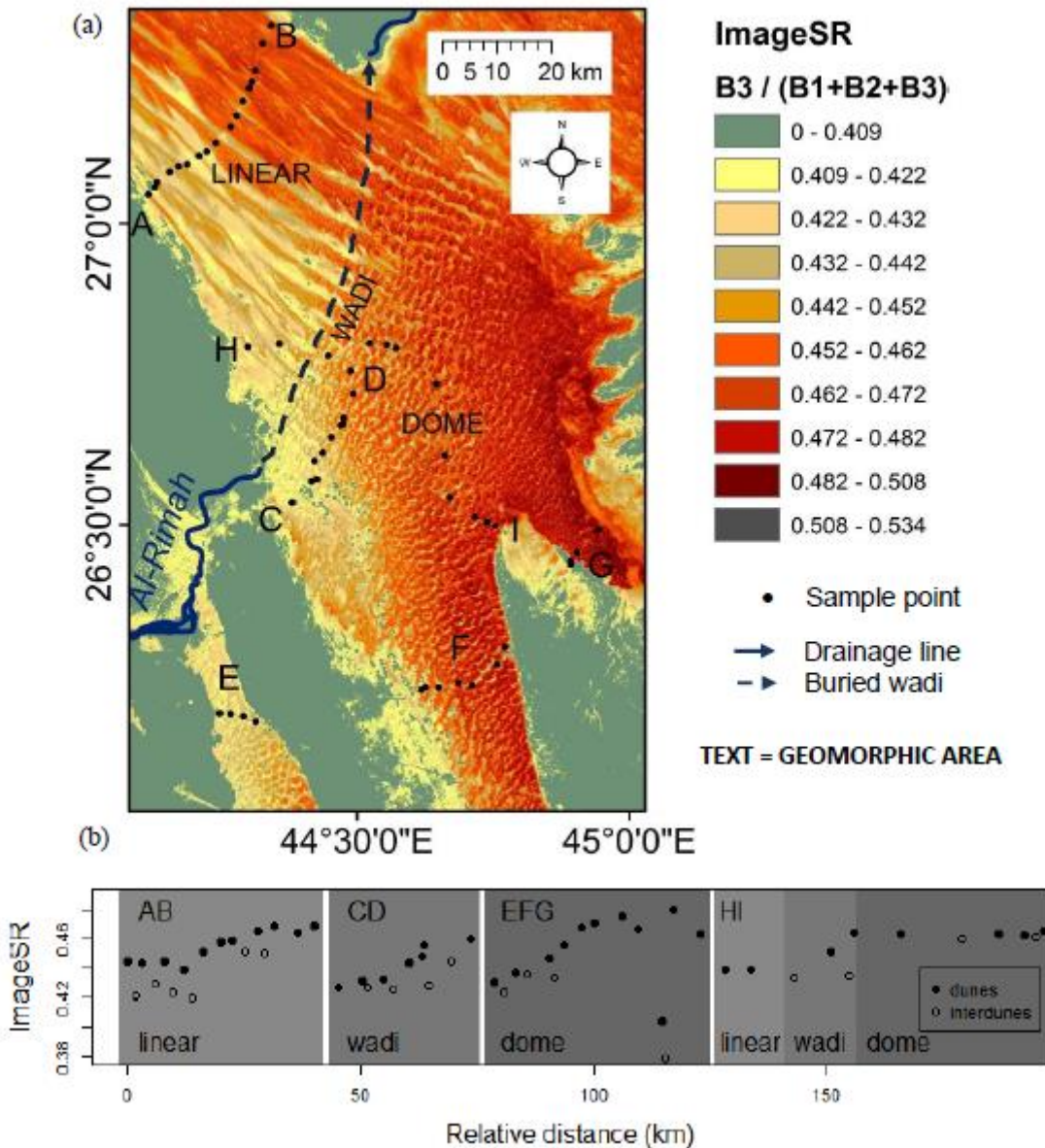


Figure 2. (a) Image Spectral Redness (ImageSR) values of the sand in the study area, with the Wadi Al-Rimah, the approximate location of the buried wadi (dashed), sample transects, and the major geomorphic areas (refer to Fig. 1 for nafud locations). (b) ImageSR values for each of the transects by geomorphic area.

Figure 3.

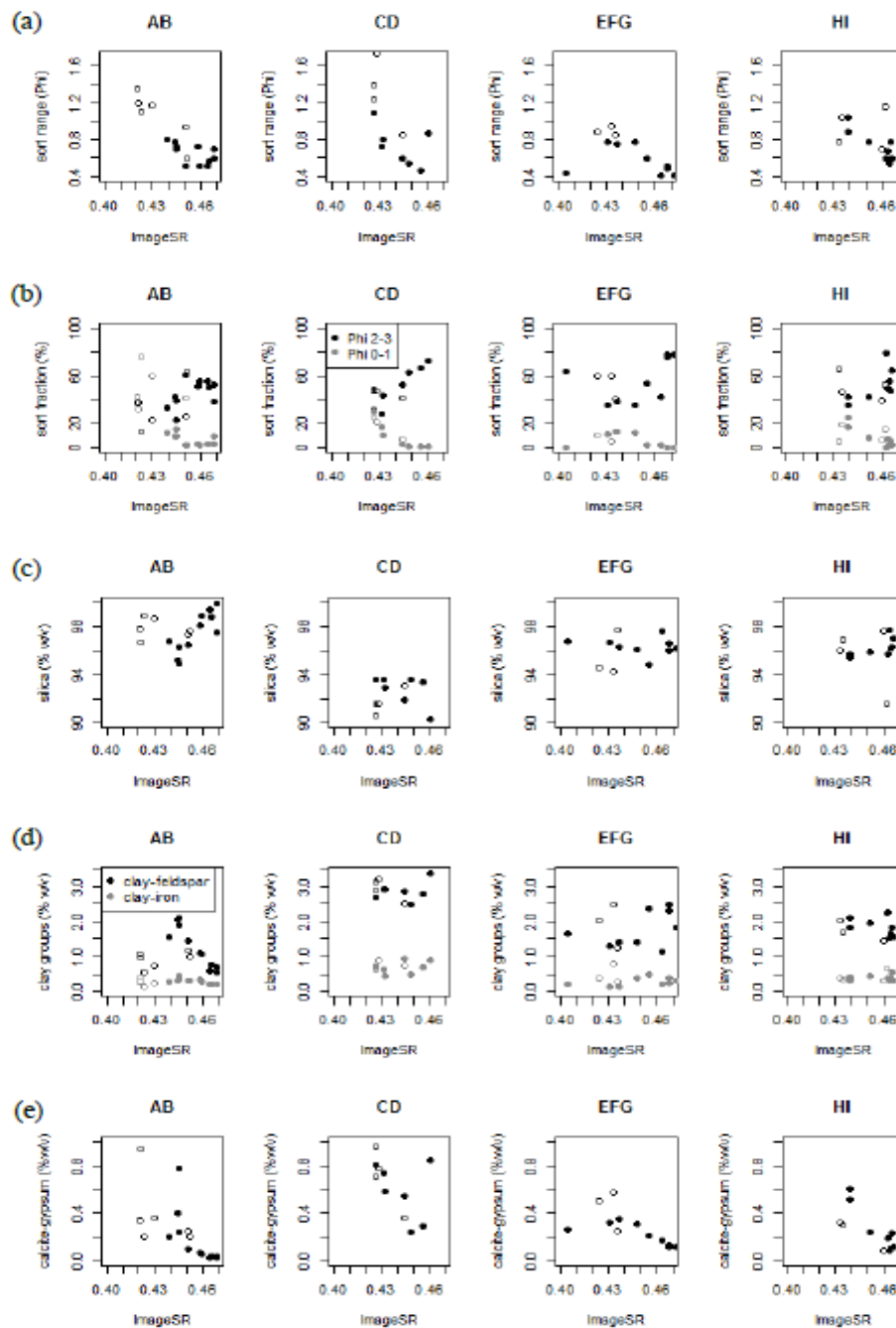


Fig. 3 (a – e). The key influences on ImageSR values for the sample transects AB, CD, EFG, HI with dunes (solid symbols) and interdunes (outlined symbols). Physical properties: (a) sorting range (ϕ); (b) fine sand, coarse sand (%); and key XRF mineralogical groups; (c) ‘Silica’ [SiO_2]; (d) ‘clay-feldspars’ [Al_2O_3] and ‘clay-iron’ [Fe_2O_3] and; (e) ‘calcite-gypsum’ [CaO] (% w/v), see text for explanation of groups.

Figure 4

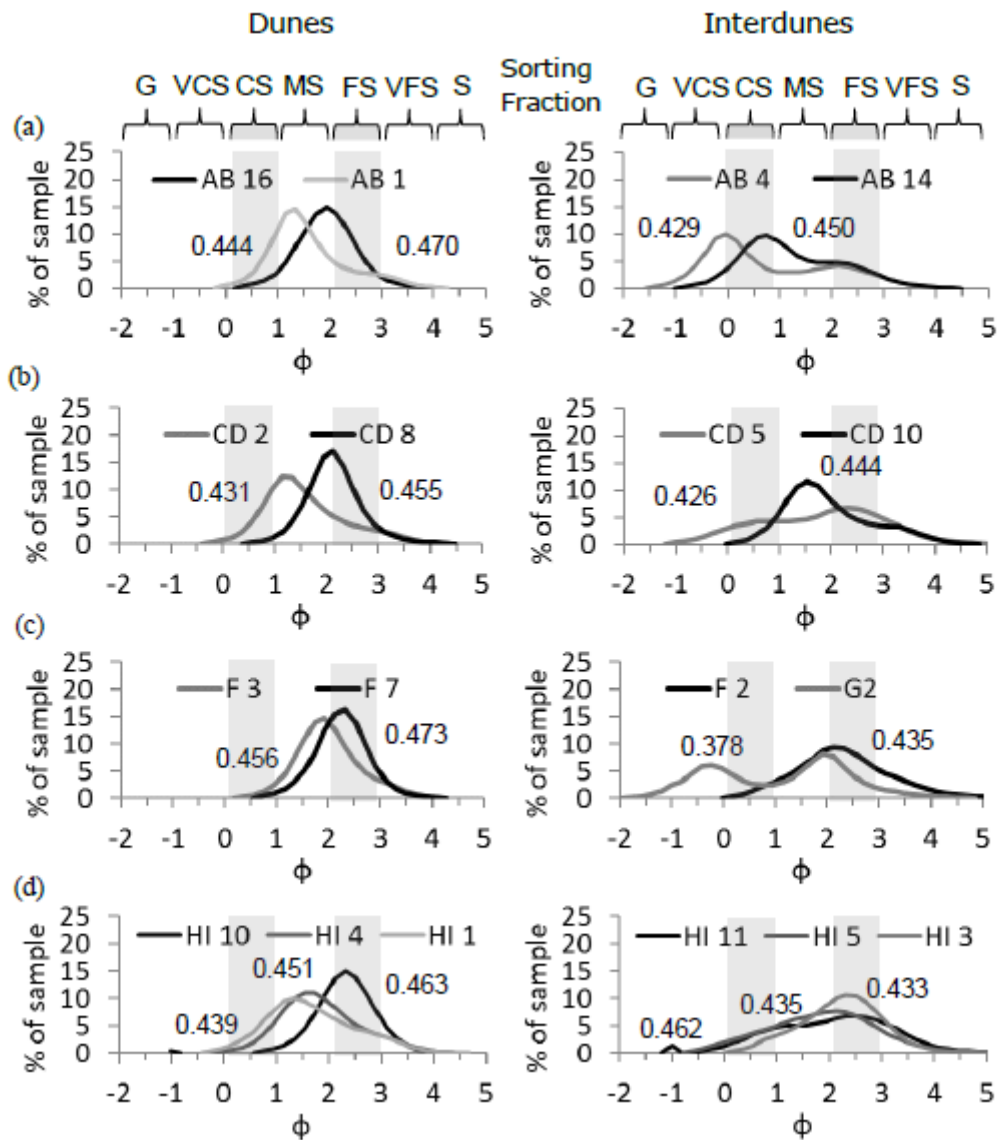


Figure 4. Selected sorting profiles for dune and interdunes representing: (a) the linear dunes - transect AB); (b) wadi - CD; (c) dome - EFG and; (d) across the linear, wadi and dome regions respectively - HI, labelled with ImageSR calculated at the sample location. Grain size category: G = granules; VCS = very-coarse-sand; CS = coarse-sand; MS = medium-sand; FS = fine-sand; VFS = very-fine-sand; SC = silt and clay. Grey highlights show the key fractions that influence colour and redness of the sands between ϕ 0 and ϕ 1, and ϕ 2 and ϕ 3.

Figure 5

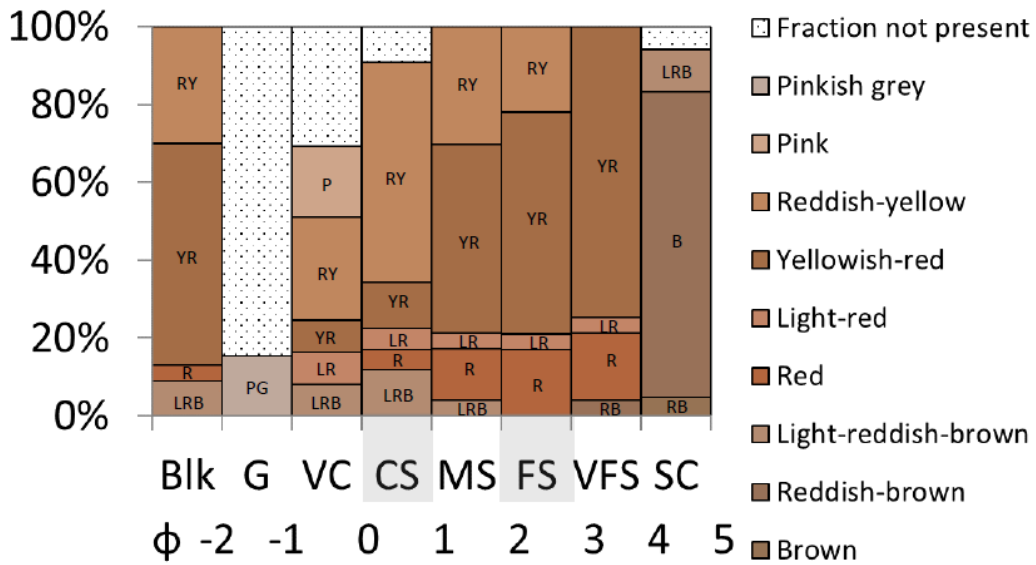


Figure. 5: The proportion of each colour identified using complete bulk (Blk) samples and the proportion of each colour of all samples after sieving into the different sorting fractions: G – Granules; VCS – Very-coarse-sand; CS – Coarse-sand; MS – Medium-sand; FS – Fine-sand; VFS – Very-fine-sand; SC – Silt and clay. Colour is measured and displayed using the true Munsell colour values (Munsell, 1975) and labelled with abbreviations for grayscale copy. Phi (ϕ) divisions are given below and the stipple shows the percentage of samples where there was no fraction after sieving. Grey highlights indicate the key sorting ranges identified to influence colour (as Fig.4).

Accepted

Figure 6

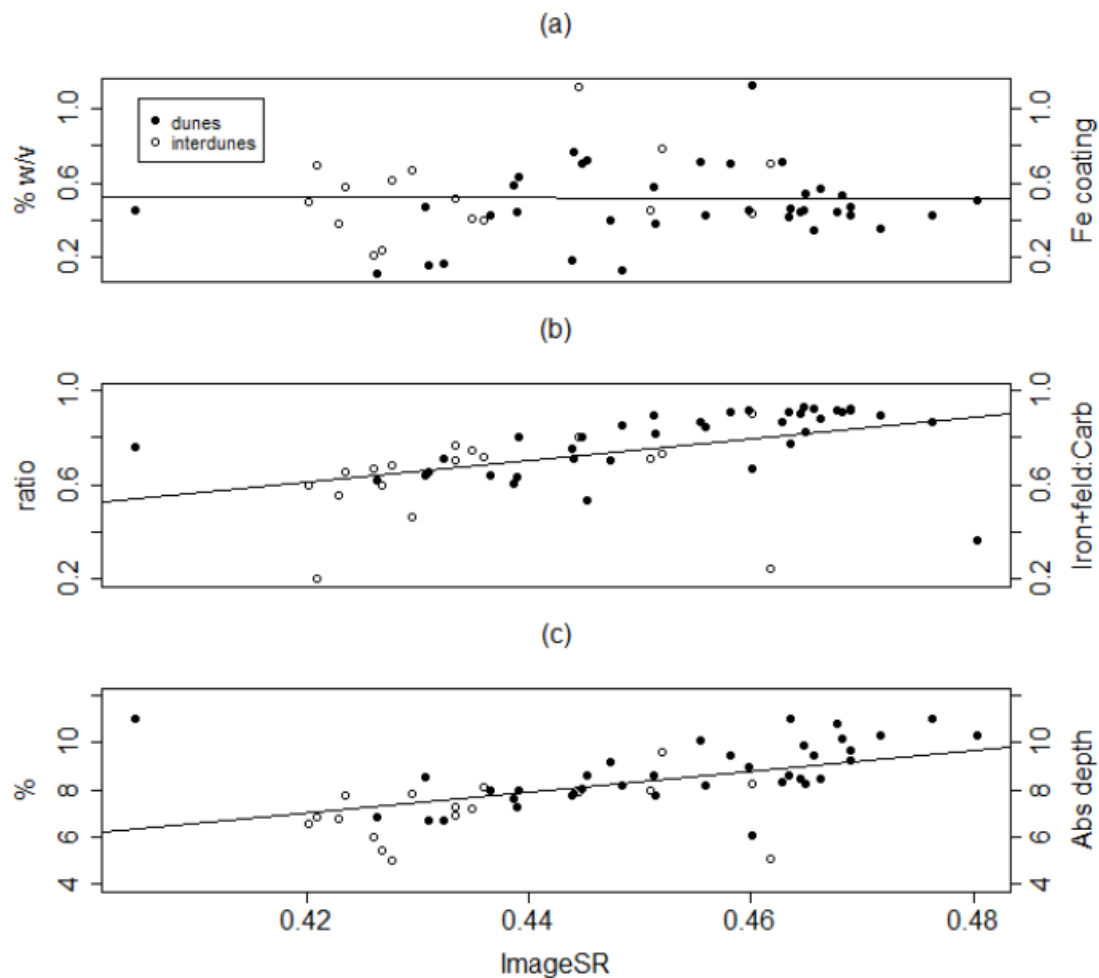


Fig. 6. ImageSR correlations with: (a) Surface extracted iron oxide (DiFe: $R_2 = <0.001$, $p = 0.90$); (b) the ratio of 'clay-feldspars' + 'clay-iron' to 'calcite-gypsum' ($R_2 = 0.27$, $p < 0.001$) and; (c) iron oxide absorption feature depth at 540 nm ($R_2 = 0.33$, $p < 0.001$).

Figure 7

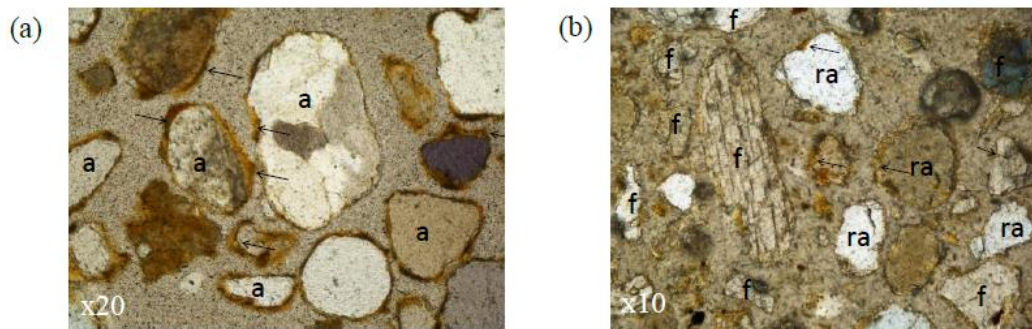


Fig. 7. (a) Nafud Dasmah within the Nafud Al-Thuwayrat. Dune sands with clay coatings and an abundance of iron oxide rims (orange-brown edges denoted by black arrows), magnification x20; (b) the edge of Wadi Al-Rimah showing a mix of dune sands and wadi sediments. The dune sands show clay coatings and thin iron oxide rims (black arrows) but the coarser angular wadi sediments do not have rims, magnification x10. Examples of: rounded aeolian clasts, a; reworked aeolian clasts, ra; and angular fluvial clasts, f, are shown.

Accepted

Figure 8

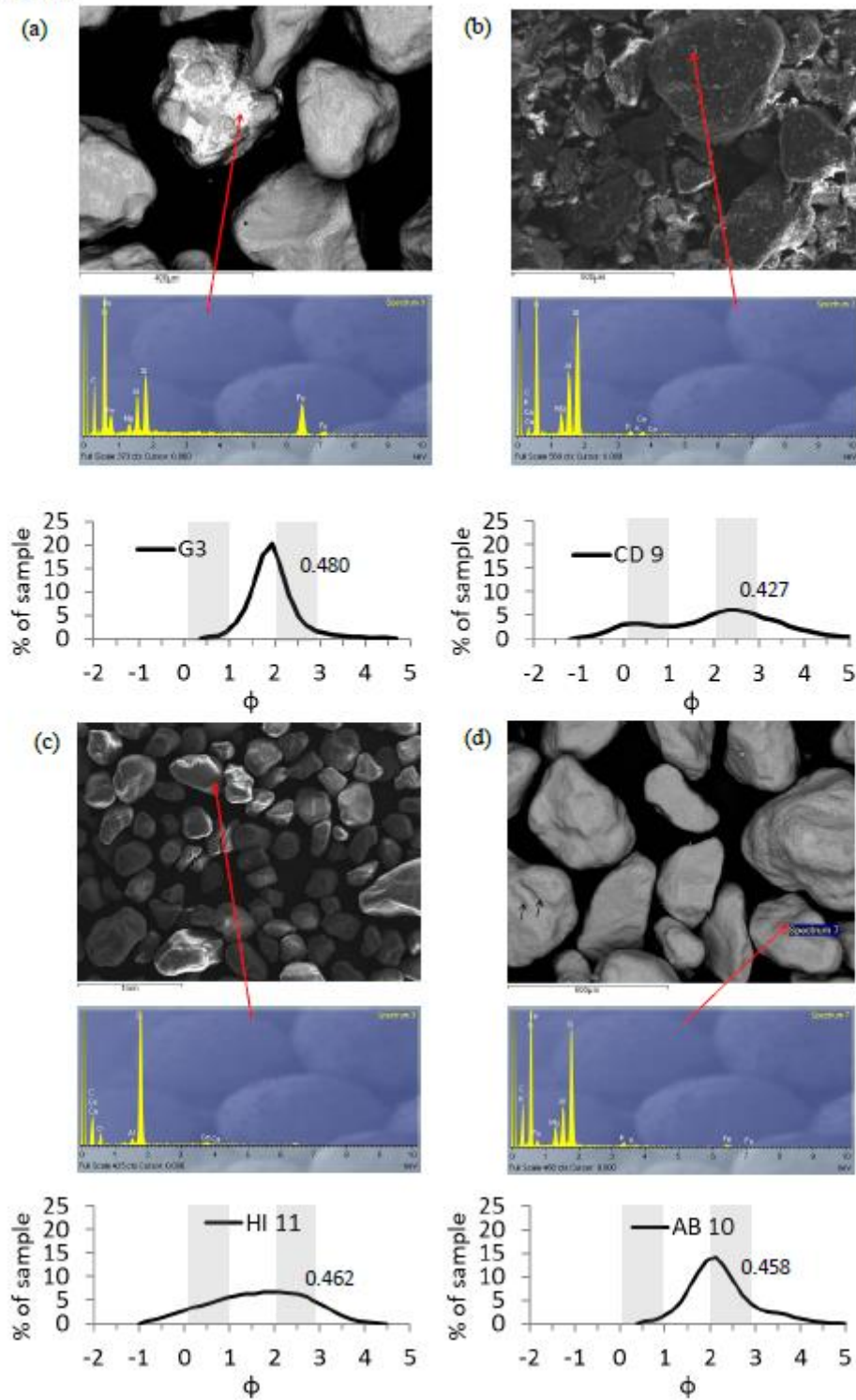


Fig. 8. Examples of SEM backscatter images with point specific EDX signatures (arrowed), and grain-size distribution from the particle size analysis with grey highlights and ImageSR corresponding to Fig. 4. (a) Transect-G3, a well-sorted dune $\sim\phi 2$. There are similar sized quartz clasts with bright areas that are identified from the EDX spectrum (Fe) as surface iron

oxide coating; (b) Transect-CD9, a poorly-sorted interdune $\sim\phi$ -1 to 4 from the wadi area. There is a mix of clast sizes and fragments coating the grains, the EDX spectrum indicates a composition of quartz (Si), feldspar, clays, and calcite (K, Al, Ca) of wadi sediments. Some dune sand grains show bright patches of iron oxide coating. (c) Transect- HI 11. An interdune between dome dunes is rich in quartz and EDX shows the presence of calcite (Ca). These grains are well rounded and sorted across a wide range of ϕ . (d) Transect-AB10 a linear dune sample. Well-rounded and sorted $\sim \phi$ 2 quartz sand grains (Si) with EDX evidence of iron oxide coatings (Fe), note the black arrows show evidence of scaling where clay platelets ought to have accumulated.

Accepted Article